Theoretical and experimental total stateselected and statetostate cross sections. III. The (Ar+H2)+ system

M. Baer, C. L. Liao, R. Xu, G. D. Flesch, S. Nourbakhsh, C. Y. Ng, and D. Neuhauser

Citation: The Journal of Chemical Physics **93**, 4845 (1990); doi: 10.1063/1.458674
View online: http://dx.doi.org/10.1063/1.458674
View Table of Contents: http://scitation.aip.org/content/aip/journal/jcp/93/7?ver=pdfcov
Published by the AIP Publishing

Theoretical and experimental total state-selected and state-to-state cross sections. III. The $(Ar+H_2)^+$ system

M. Baer,[a] C.-L. Liao, R. Xu, G. D. Flesch, S. Nourbakhsh, and C. Y. Ng
Ames Laboratory, U. S. Department of Energy and Department of Chemistry, Iowa State University, Ames, Iowa 50011

D. Neuhauser[b]
Department of Chemistry, Princeton University, Princeton, New Jersey 08544

(Received 8 March 1990; accepted 18 June 1990)

A detailed three-dimensional quantum mechanical study of the $(Ar + H_2)^+$ system along the energy range 0.4 eV$\leqslant E_{tot} \leqslant$1.65 eV is presented. The main difference between this new treatment and the previously published one [J. Chem. Phys. **87**, 465 (1987)] is the employment of a new version of the reactive infinite-order sudden approximation (IOSA), which is based on the ordinary inelastic IOSA carried out for an optical potential. In the numerical treatment we include three surfaces (only two were included in the previous treatment), one which correlates with the $Ar + H_2^+$ system and two which correlate with the two spin states of Ar^+ (^2P_j); $j = 3/2,1/2$. The results are compared with both trajectory-surface-hopping calculations and with experiments. In most cases, very good agreement is obtained.

I. INTRODUCTION

This is the third time that the $(Ar + H_2)^+$ system is being exposed to a quantum mechanical study. There are two main reasons for doing this: (1) New experimental studies have been carried out by us and, for the first time, absolute vibronic state-to-state charge transfer and spin transition cross sections have been obtained.[1,2] (2) A new approach to treating exchange collisions has recently been introduced,[3–9] and it seems likely that the corresponding reactive infinite-order sudden approximation (RIOSA) will yield better results than those obtained using the previous version.

The $(Ar + H_2)^+$ system is unique in that, on the one hand, it contains all possible competing processes that may occur in an ion (atom)–diatomic molecule (ion) collision, ranging from vib-rotational (inelastic) transitions through charge transfer and spin flip transitions to chemical reactions and dissociations. On the other hand it is simple enough to be treated quantum mechanically.

The new approach, recently introduced to treat exchange collisions, is based on employing short-range negative imaginary potentials[3] (termed optical potentials throughout this paper) to convert a multi-arrangement system into an inelastic single-arrangement system. It is found that by doing so one obtains not only the correct inelastic transition probabilities but also the correct total (and sometimes even state-to-state) transition probabilities for the various ignored products arrangements. This conversion is done by substituting these potentials at the entrances of all exchange arrangements. However, they must be located deep enough into each arrangement so that they absorb outgoing fluxes only. A valuable feature about the negative imaginary potentials is that they do not affect the wave function in the regions external to them, but once the wave function passes through them, it decays to zero within a short distance.

So far, we have treated various collinear[4,6(a),9] and three-dimensional systems.[5,6(b),7,8] These treatments were carried out within the time-dependent wave packet framework[3–5,7] and the time-independent framework.[6,8,9] Here we emphasize the time-independent study that was performed on the collinear $H + H_2$ system.[9] In that study two subjects are addressed: (a) *The Schrödinger equation* which results from our treatment and contains the optical potential is shown to be solved without difficulty by propagating the wave function (or eventually other functions, such as the **S** matrix[10]) from the origin out to the asymptotic region; and (b) *the parameters of the optical potential* are determined *a priori*, based on analytic arguments, and the calculated transition probabilities are shown to be stable against reasonable variations of these parameters.

The RIOSA consists of collinear-type configurations.[11–15] Our previous version[11] is based on a transformation from reagents to products coordinates, assuming the transition from one arrangement to the other takes place on a surface which separates the two arrangements. This procedure, when applied to the $(Ar + H_2)^+$ system,[16] is found to yield reactive cross sections far too small compared to both the experimental cross sections[17,18] and the cross sections obtained by the semiclassical trajectory-surface-hopping (TSH) calculation.[19] The reason is not entirely clear (we discuss this to a certain extent in Sec. V). In the new RIOSA version applied here,[20] the incorporation of the optical potentials enables us to consider this system as inelastic, and therefore the transformation from one set of coordinates to another (which seemed to be the reason for the too small reactive cross sections) becomes unnecessary. In the present study we examine whether this new version of the RIOSA

[a] Visiting Professor. Permanent address: Department of Physics and Applied Mathematics, Soreq Nuclear Research Center, Yavne 70600, Israel.
[b] Recipient of the Weizmann Postdoctoral Fellowship, 1989–1990.

 0021-9606/90/194845-13$03.00

yields better reactive cross sections than those of the previous one.

The question, whether an IOSA treatment for charge transfer is at all relevant for the mass combination exhibited by the $(Ar + H_2)^+$ system, is a valid one. In fact, it has been argued in the literature (based on numerical experience) that the IOSA is useful mainly for a light-heavy-heavy mass combination.[21] This numerical "evidence" must be strongly potential-dependent. For instance, the IOSA becomes exact for a breathing sphere type potential, irrespective of the masses. Therefore it is expected, in case of a quasi-isotropic potential (such as that usually encountered in ion–molecule collisions), to be appropriate for any mass combination.[16,22,23] The best example is the recent $(H + H_2)^+$ study for which good agreement with experiment has been obtained.[22]

The theoretical–numerical study of the $(Ar + H_2)^+$ system is based on the 6×6 DIM potential energy matrix derived by Kuntz and Roach[24] and slightly modified by Chapman.[19] So far, all dynamical calculations, with the exception of a simplified model treatment by Tanaka *et al.*,[17] have been carried out with respect to the two lowest adiabatic potential energy surfaces: the adiabatic potential energy surface correlating asymptotically with $Ar + H_2^+$; and an average of two surfaces that asymptotically correlates with the average of the $Ar^+(^2P_{3/2}) + H_2$ and the $Ar^+(^2P_{1/2}) + H_2$ systems. Here, for the first time in an extensive calculation, we distinguish between the two spin states of Ar^+, and consequently the numerical study is carried out employing *three* surfaces. The details of the incorporation of the two spin states in the DIM matrix are given in Paper I of this series (where we followed a procedure by Tanaka *et al.*[17]).

This paper is organized as follows: Section II is theoretical and in it the old and new versions of the RIOSA are briefly compared. In Sec. III we discuss numerical aspects of the new RIOSA. Section IV presents a detailed comparison between theoretical and experimental initial state-selected total and state-to-state integral cross sections and in Sec. V we discuss the comparison and analyze the results. A summary is given in Sec. VI.

II. THEORY

A. Introductory remarks

Our theory for treating charge transfer processes is usually divided into two parts. First, we consider the potential and the changes to be made in order to guarantee a stable solution of the Schrödinger equation (SE). Then we construct the relevant SE and describe the incorporated approximations. Both parts have been treated a number of times in our previous publications.[16,25] In Paper I of this three-part series we describe in detail the modifications relevant for the calculations of the two spin states of $Ar^+(^2P_j)$, which is used in this paper, and we shall not repeat those details here.

The emphasis in this theoretical section is on the reactive channel and how it is treated within the IOSA. Before describing the new version of the reactive IOSA (RIOSA) employed in this paper, let us briefly review the previous version.

B. The previous version of the RIOSA

Within the framework of the previous RIOSA we consider two arrangement channels, one with respect to the reagents (λ) and the other to the products (ν). Each is treated separately and consequently two collinear-type SE's, Eq. (1), are considered (in this discussion we treat the single-surface case only),

$$\left\{-\frac{\hbar^2}{2\mu}\nabla_\alpha^2+\frac{\hbar^2}{2\mu}\frac{l_\alpha(l_\alpha+1)}{R^2}+\frac{\hbar^2}{2\mu}\frac{j_\alpha(j_\alpha+1)}{r^2}+V(R_\alpha,r_\alpha;\gamma_\alpha)-E\right\}\psi_\alpha(R_\alpha,r_\alpha;\gamma_\alpha)=0,\quad \alpha=\lambda,\nu \tag{1}$$

where R_α and r_α are the translational and vibrational coordinates, γ_α is the IOSA angle defined as

$$\gamma_\alpha=\cos(\hat{R}_\alpha\cdot\hat{r}_\alpha), \tag{2}$$

l_α and j_α are the orbital and the internal angular momentum quantum numbers, ∇_α^2 is the corresponding Laplacian, and λ and ν are the two arrangement channels to be considered. Once all the independent solutions of the two SE's are available, a linear combination of each of them is matched to form the required physical solution. The matching is done along a straight line which follows from the relation

$$r_\nu=Br_\lambda, \tag{3}$$

where $B(\gamma_\lambda,\gamma_\nu)$ is a constant that is determined uniquely for each pair of angles $(\gamma_\lambda,\gamma_\nu)$. The leading idea behind this version of the RIOSA is that the reagents and products are moving on two different planes: the reagents plane formed by holding γ_λ fixed, and the products plane formed by holding γ_ν fixed. It has been proven that the two planes intersect along a straight line which goes through the origin[11(b)] The tangent of this line follows from Eq. (3). Whereas this approach yields reasonable relative cross sections, their absolute values are not always satisfactory. In some cases [such as $F + H_2$ (Ref. 26) or $Ar + H_2^+$ (Ref. 16)] the cross sections at the higher energy regions are too small, while in other cases [such as $H + D_2$ (Ref. 27)], again at the higher energy region, the cross sections are too large. No obvious explanation can be given for these two different observations.

C. The new RIOSA: Application of optical potentials

Within the framework of the new RIOSA, only the reagents arrangement channel is considered. The other arrangements are eliminated, as will be explained, by the use of optical potentials. As mentioned in the Introduction, these potentials have been successfully employed in both collinear and three-dimensional cases. The fact that the reagents arrangements can be ignored enables application of the ordinary inelastic (nonreactive) IOSA[21] without having to consider the other arrangements. However, this does not mean that reactive cross sections cannot be obtained. On the contrary, as in our exact three-dimensional treatment, we still calculate integral total reactive cross sections and, as will be

shown, they fit reasonably well with both the TSH and the experimental cross sections.

The treatment of an inelastic collision within the IOSA is well known and is not repeated here (for the treatment of a charge transfer process for an inelastic system within the IOSA, see Ref. 22). The only difference between the ordinary inelastic treatment and the treatment suggested here is in the application of the optical potential.[3] Therefore the rest of this section is devoted to this subject.

Within the reactive IOSA one considers collinear-type configurations and therefore, for the sake of simplicity, we discuss the reactive collinear system described in Fig. 1. The short-range optical potential $u_I(R,r)$ is located in the shadowed area.

A convenient form for such a potential is given by Eq. (4),

$$u_I(R,r;\gamma)=\begin{cases} -iu_{I0}(\gamma)\dfrac{r-r_{1I}}{r_{2I}-r_{1I}}; & r_{1I}\leqslant r\leqslant r_{2I} \\ 0; & \text{otherwise} \end{cases}, \tag{4}$$

where the region for R is unlimited and $u_{I0}(\gamma)$ must fulfill the two inequalities:

$$\hbar E_{CM}^{1/2}/(\Delta r_I\sqrt{8m}) \ll u_{I0}(\gamma) \ll \Delta r_I\sqrt{8m}E_{CM}^{3/2}/\hbar. \tag{5}$$

Here E_{CM} is the translational energy of the system interacting with the optical potential, m is its mass, and Δr_I is its nonzero range:

$$\Delta r_I = r_{2I}-r_{1I}. \tag{6}$$

In Eq. (5), the left-hand inequality guarantees that all the flux passing through this potential is absorbed and the right-hand inequality guarantees that no flux is reflected while passing through it. Once this potential is given, we add it to the potential which governs the motion of the interacting particles and consider the sum as an ordinary potential.

Since we must treat only one arrangement channel, the corresponding IOSA SE to be solved is

$$\left(-\frac{\hbar^2}{2\mu}\nabla^2+\frac{\hbar^2}{2\mu}\frac{l(l+1)}{R^2}+\frac{\hbar^2}{2\mu}\frac{j(j+1)}{r^2}+V_c(R,r;\gamma)-E\right)\psi(R,r;\gamma)=0, \tag{7}$$

where $V_c(R,r;\gamma)$ is the modified interaction potential given in the form

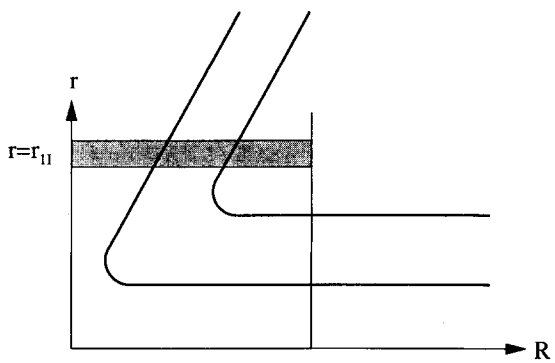

FIG. 1. The collinear-type mass-scaled potential energy surface. The negative absorbing potential is located along $r=r_{1I}$.

$$V_c(R,r;\gamma)=V(R,r;\gamma)+u_I(R,r;\gamma). \tag{8}$$

In case of a multi-surface system [see Paper I in this series, Eq. (4.9)], the pseudo-inelastic SE to be solved is Eq. (9),

$$\left(-\frac{\hbar^2}{2\mu}\nabla^2+\frac{\hbar^2}{2\mu}\frac{l(l+1)}{R^2}+\frac{\hbar^2}{2\mu}\frac{j(j+1)}{r^2}-E\right)\Psi_i+\mathbf{W}_{ci}^{(n)}\Psi=0, \quad i=1,\ldots,n \tag{9}$$

where $\mathbf{W}_c^{(n)}$ is the diabatic potential energy matrix of order $n\times n$.

In the particular case of the present $(Ar+H_2)^+$ system we consider a three-surface system, the lowest surface of which, namely, $W_1(R,r;\gamma)$, is reactive. Consequently, $u_I(R,r;\gamma)$ is added to $W_1(R,r;\gamma)$ only, and the rest of the original $\mathbf{W}^{(n)}$ matrix is left unchanged.

In a previous publication, we described in detail how an equation similar to Eq. (7) is solved by propagation.[9] Employing the same method, we solve the (multi-surface) system of equations presented in Eq. (9). No further details are given here.

The solution of Eq. (9) yields S matrix elements of the form $S(E,\gamma,l\,|q_i,v_i,q_f,v_f)$, where E, γ, and l were introduced earlier, q_i and q_f stand for the initial and final electronic states, respectively, and v_i and v_f are the corresponding initial and final vibrational states. The fact that the interaction potential contains an imaginary component does not affect the hermitian property of the S matrix, but it may destroy its unitarity. The nonunitarity is related to the fact that the interaction may lead to exchange. Consequently, $P_r(E,\gamma,l\,|q_i,v_i)$, the reaction probability for a given initial state (q_i,v_i), is calculated from the expression

$$P_r(E,\gamma,l\,|q_i,v_i)=1-\sum_{q_f v_f}|S(E,\gamma,l\,|q_i,v_i,q_f,v_f)|^2, \tag{10}$$

where the summation is carried out with respect to all (asymptotic) open states.

In this work we consider four types of cross sections.

(a) Differential total (nonreactive) cross sections:

$$\frac{d\sigma(E\,|q_i,v_i,q_f)}{d\Omega}=\frac{1}{8k_{q_iv_i}^2}\sum_{l=0}^{l_m}\sum_{l'=0}^{l_m}(2l+1)(2l'+1)P_l(\cos\theta)\times P_{l'}(\cos\theta)\sum_{v_f}\int_{-1}^{+1}d(\cos\gamma)S(E,\gamma,l\,|q_i,v_i,q_f,v_f)\times S^*(E,\gamma,l'\,|q_i,v_i,q_f,v_f). \tag{11}$$

Here $P_l(\cos\theta)$ is the l-th Legendre polynomial, θ is the scattering angle, and $k_{q_iv_i}$ is the wave vector defined as

$$k_{q_iv_i}=\sqrt{2\mu(E-E_{q_iv_i})}/\hbar, \tag{12}$$

where $E_{q_iv_i}$ is the initial vib-electronic eigenvalue.

(b) State-to-state (nonreactive) integral cross sections:

$$\sigma(E\,|q_i,v_i,q_f,v_f) = \frac{\pi}{2k^2_{q_iv_i}} \sum_{l=0}^{l_m} (2l+1) \times \int_{-1}^{+1} d(\cos\gamma)\,|S(E,\gamma,l\,|q_i,v_i,q_f,v_f)|^2 \tag{13}$$

and initial total reactive cross sections

$$\sigma_r(E\,|q_i,v_i) = \frac{\pi}{k^2_{q_iv_i}}(l_m+1)^2 - \sum_{q_fv_f} \sigma(E\,|q_i,v_i,q_f,v_f), \tag{14}$$

where $\sigma(E\,|q_i,v_i,q_f,v_f)$ is defined in Eq. (13).

(c) Initial state (nonreactive) opacity functions:

$$P(E,l\,|q_i,v_i,q_f) = \sum_{v_f} \frac{1}{2} \int_{-1}^{+1} d(\cos\gamma)\,|S(E,\gamma,l\,|q_i,v_i,q_f,v_f)|^2 \tag{15}$$

and the corresponding reactive functions

$$P_r(E,l\,|q_i,v_i) = 1 - \sum_{q_f} P(R_t,l\,|q_i,v_i,q_f), \tag{16}$$

where $P(E,l\,|q_i,v_i,q_f)$ is defined in Eq. (15).

(d) γ-dependent initial state (nonreactive) cross sections:

$$\sigma(E,\gamma|q_i,v_i,q_f) = \frac{\pi}{k^2_{q_iv_i}} \sum_{l=0}^{l_m} (2l+1) \times \sum_{v_f} |S(E,\gamma,l\,|q_i,v_i,q_f,v_f)|^2 \tag{17}$$

the corresponding reactive cross sections:

$$\sigma_r(E,\gamma|q_i,v_i) = \frac{\pi}{k^2_{q_iv_i}}(l_m+1)^2 - \sum_{q_f} \sigma(E,\gamma|q_i,v_i,q_f), \tag{18}$$

where $\sigma(E,\gamma|q_i,v_i,q_f)$ is defined as Eq. (17).

This completes our theoretical section.

III. THE NUMERICAL TREATMENT

Our main concern in the numerical treatment is the parameters defining the optical potential. In a previous publication[9] we showed how they are determined *a priori*, using the inequalities of Eq. (5). Here, we follow the same procedure and calculate the coefficients shown in Table I. It is noticed that the coefficients vary with γ (but not with l). The reason is that the extent to which the product ArH^+ is excited is strongly dependent on γ, as was shown in our previous RIOSA study for this system.[16] Thus, the fact that the products are highly excited enforces the use of relative small values of u_{I0} to avoid reflection before the resulting slowly moving wave function penetrates the complex potential. On the other hand, when γ is large enough, the products are only slightly excited and relatively large values of u_{I0} can be employed. In Fig. 2 we present γ-dependent cross sections as a function of u_{I0} for both the exchange and the charge transfer processes. The results were obtained for $E_{tot} = 1.435$ eV, and we show those for $\gamma = 30°$ and for $\gamma = 60°$. Note that along a relatively large range of u_{I0} the results hardly change and when they do change, they usually attain their maximal value within the indicated range.

TABLE I. Dependence of u_{I0} on the orientation angle γ.

γ	0°	15°	30°	45°	60°	75°	90°
u_{I0} [a]	0.7	0.7	0.7	1.2	2.0	2.0	2.0

[a] Values are in eV.

The actual calculations have been carried out for six values of E_{tot}: 0.4, 0.65, 0.90, 1.145, 1.435, and 1.650 eV. Since at each total energy we have several open initial states, and consequently several initial translational energies, we collect them in Table II for those reagents of interest.

The calculations were carried out for 7 equidistant values of γ, with $\Delta\gamma = 15°$. At each γ value, the three coupled SE were solved for every l value at $E_{tot} = 0.4$; for every second l value at $E_{tot} = 0.65$, 0.9, and 1.145 eV; and for every third l value at $E_{tot} = 1.65$ eV. For $E_{tot} = 1.435$ eV, the SE's were solved again for every l value, in order to obtain correct differential cross sections and to check accuracies.

In order to obtain reliable results, we had to include closed vibrational channels. Depending on E_{tot}, we usually included between 10 and 15 vibrational states for the lower surface, and between 8 and 12 vibrational states for the two upper surfaces.

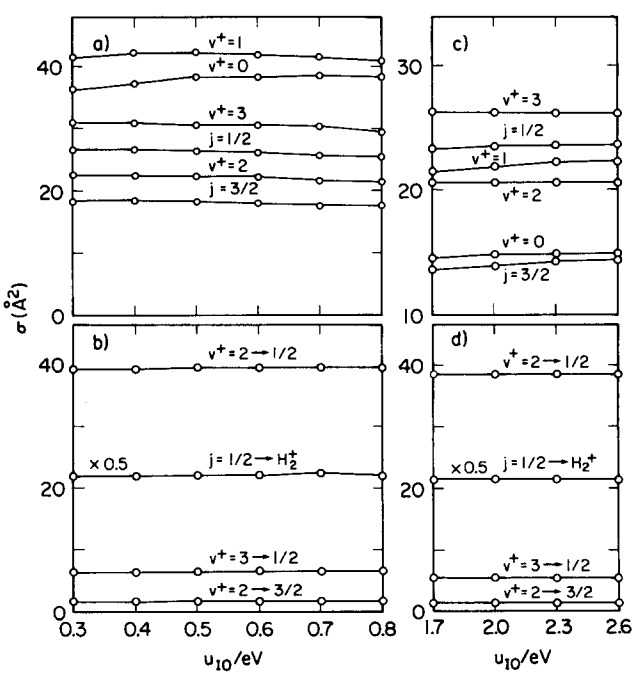

FIG. 2. The dependence of the orientation-angle–dependent cross sections $\sigma(\gamma)$ on the complex potential parameter u_{I0}, as obtained for $E_{tot} = 1.435$ eV. The results in (a) and (c) are for the exchange process (the symbol v^+ stands for the reaction $H_2^+(v^+) + Ar \rightarrow ArH^+ + H$ and the symbol j stands for the reaction $Ar^+(^2P_j) + H_2 \rightarrow ArH^+ + H$). The results in (b) and (d) are for the charge transfer process (the symbol $v^+ \rightarrow j$ stands for the process $Ar^+H_2^+(v^+) \rightarrow Ar^+(^2P_j) + H_2$ and the symbol $j \rightarrow H_2^+$ stands for the process $Ar^+(^2P_j) + H_2 \rightarrow Ar + H_2^+$). The results in (a) and (b) are for $\gamma = 30°$ and those in (c) and (d) are for $\gamma = 60°$.

TABLE II. Relations between total and translational energies (eV).

	$Ar + H_2^+(v^+)$					$Ar^+(^2P_j) + H_2(v=0)$	
State	0	1	2	3	4	3/2	1/2
$E_{tot} \setminus E_{vib}$	0.146	0.424	0.685	0.928	1.154	0.489	0.669
0.400	0.254	...	...	...	...	...	...
0.650	0.504	0.226	...	...	...	0.161	...
0.900	0.754	0.476	0.215	...	...	0.411	0.233
1.145	0.999	0.721	0.460	0.217	...	0.656	0.478
1.435	1.289	1.011	0.750	0.507	0.281	0.946	0.768
1.650	1.504	1.226	0.965	0.722	0.496	1.161	0.983

IV. RESULTS: COMPARISON BETWEEN THEORY AND EXPERIMENT

Here we distinguish five kinds of results: exchange (reactive) processes with $Ar + H_2^+(v^+)$ and $Ar^+(^2P_j) + H_2(v=0)$, respectively, as reagents; charge transfer processes, again with the above two kinds of reagents; and spin transitions, i.e.,

$$Ar^+(^2P_{1/2}) + H_2 \rightleftarrows Ar^+(^2P_{3/2}) + H_2. \quad (I)$$

All the calculated results have been compared with experimental results obtained in this laboratory and elsewhere, as well as with other theoretical results. The various results are summarized in Tables III–VI and in Figs. 3–17.

A. Results for $Ar+H_2^+(v^+) \rightarrow ArH^+ + H$

The initial state-selected total cross sections for these processes are presented in Table III and in Figs. 3 and 4. The dependence on v^+ for several translational energies E_{CM} is shown in Fig. 3, and the dependence on E_{CM} for various v^+ states in Fig. 4. In Fig. 3(a) the IOSA cross sections for $E_{CM} = 0.48$ eV are compared with experimental results obtained in our laboratory and by Tanaka *et al.*[17,18] It is seen that the features found in the experiment are nicely reproduced by the IOSA calculation, in particular, the strong dip at $v^+ = 2$ and the shoulder at $v^+ = 1$. It is important to emphasize that here and elsewhere, unless otherwise specified, the comparison is between absolute values for both theory and experiment, and therefore no normalization factors have been used. The theoretical IOSA cross sections are compared with Tanaka *et al.*'s[17,18] results for $E_{CM} = 0.75$ eV in Fig. 3(b). Again, a reasonably good fit is obtained. Energy-dependent cross sections for $v^+ = 0,1,2$ are presented in Figs. 4(a), 4(b), and 4(c), respectively. It is seen that for $v^+ = 0,1$ the fit among the different kinds of results is quite good. Note that, as far as the present version of the

TABLE III. Exchange cross sections (Å^2) for the reactions $Ar + H_2^+(v^+) \rightarrow ArH^+ + H$.

Translational energy (eV)	v^+	0	1	2	3	4
0.22	$T1$[a]	36.1	46.2	2.9	17.2	24.8
	$T2$	...	20.0	...	...	...
	$T3$	...	37.0	...	...	...
0.48	$T1$	24.5	32.8	12.9	27.4	28.0
	$T2$	8.8	...	...	...	...
	$T3$	31.0	...	...	...	...
	$E1$	27.0 ± 1.4	31.0 ± 1.6	22.5 ± 1.5	26.5 ± 1.8	28.0 ± 3.2
	$E2$	27.4	34.0	21.3	32.3	36.4
0.75	$T1$	17.8	26.4	19.9	29.7	...
	$E2$	22.6 ± 4.7	24.5 ± 4.7	28.0 ± 4.7	26.6 ± 4.7	32.8 ± 4.7
1.00	$T1$	17.8	23.1	22.0	...	...
	$T3$	15.0 ± 1.3	28.6 ± 3.1	26.2 ± 2.9	...	22.5 ± 2.6
	$E1$	25.6 ± 1.3	28.0 ± 1.4	22.0 ± 1.5	23.3 ± 1.6	25.0 ± 3.7
	$E3$	51.8	66.1	69.1	67.7	73.4
1.30	$T1$	16.4	21.7	...	...	...
	$E2$	21.5 ± 5.4	23.6 ± 5.4	26.0 ± 5.4	$31.8 - 5.4$	25.4 ± 5.4
1.50	$T1$	15.3	...	...	...	...

[a] $T1$, Present complex RIOSA; $T2$, previous RIOSA (Ref. 16); $T3$, TSH (Ref. 19); $E1$, present experimental; $E2$, Tanaka *et al.* (Refs. 17 and 18); $E3$, Houle *et al.* (Ref. 29).

TABLE IV. Charge transfer cross sections (Å^2) for the process $Ar + H_2^+(v^+) \rightarrow Ar^+ + H_2$.

Translational energy (eV)	v^+	0	1	2	3	4
0.22	$T1$[a]	Closed	1.7	17.2	7.5	10.8
	$T2$	Closed	24.0	...	...	...
	$T3$	Closed	31.0	...	...	...
0.48	$T1$	0.2	3.3	31.2	7.7	12.0
	$T2$	2.6	...	...	...	...
	$T3$	0.8	...	...	...	...
	$E1$	2.0 ± 0.1	5.3 ± 0.3	27.5 ± 2.0	14.6 ± 0.9	13.6 ± 2.1
	$E2$	0.0 ± 2.8	3.3 ± 2.8	25.9 ± 2.8	10.8 ± 2.8	6.9 ± 2.8
0.75	$T1$	0.7	4.2	40.5	8.3	...
	$E2$	0.3 ± 2.6	3.6 ± 2.3	25.8 ± 2.6	14.2 ± 2.6	9.6 ± 2.6
1.00	$T1$	0.6	6.6	44.0	...	...
	$T3$	1.9 ± 0.5	28.6 ± 3.1	22.4 ± 3.6	...	21.1 ± 3.6
	$E1$	2.0 ± 0.1	5.9 ± 0.3	27.0 ± 1.9	15.5 ± 1.1	11.7 ± 1.8
	$E3$	3.1	17.7	47.2	28.4	24.4
1.25	$T1$	0.8	7.1	...	...	...
	$E2$	1.0 ± 3.4	6.4 ± 3.4	28.4 ± 3.4	16.9 ± 3.4	9.4 ± 3.4
1.5	$T1$	0.9	...	...	...	...

[a] $T1$, present RIOSA; $T2$, previous RIOSA (Ref. 16); $T3$, TSH (Ref. 19); $E1$, present experimental; $E2$ Tanaka *et al.* (Refs. 17 and 18); $E3$, Houle *et al.* (Ref. 29).

TABLE V. State-to-state charge transfer cross sections (Å^2) for $Ar + H_2^+(v^+) \rightarrow Ar^+(^2P_j) + H_2$.

Translational energy (eV)		j v^+	0	1	2	3	4
0.22	T[a]	3/2	Closed	1.7	0.5	1.1	5.8
	E	3/2	Closed	...	...	...	...
	T	1/2	Closed	Closed	17.1	6.4	5.0
	E	1/2	Closed	Closed	...	...	...
0.48	T	3/2	0.2	3.1	1.0	1.6	5.4
	E	3/2	2.0 ± 0.1	5.3 ± 0.4	6.0 ± 0.5	4 ± 3	4 ± 3
	T	1/2	Closed	0.2	30.6	6.1	5.0
	E	1/2	Closed	0.0	21.5 ± 1.5	11 ± 3	10 ± 3
0.75	T	3/2	0.6	3.8	1.8	0.9	...
	E	3/2	...	...	...	...	...
	T	1/2	0.03	0.4	38.7	6.3	...
	E	1/2	...	...	...	...	...
1.00	T	3/2	0.6	6.2	3.0	...	...
	E	3/2	2.0 ± 0.1	5.9 ± 0.4	6.3 ± 0.6	4 ± 1.5	8.2 ± 3.5
	T	1/2	0.07	0.4	40.8	...	...
	E	1/2	0.0	0.0	21.3 ± 1.5	11.5 ± 1.5	3.5 ± 3.5
1.25	T	3/2	0.6	6.8	...	...	...
	T	1/2	0.1	0.5	...	...	...
1.50	T	3/2	0.8	...	...	...	...
	T	1/2	0.1	...	...	...	...

[a] T, Present RIOSA; E, present experimental.

TABLE VI. Spin transition cross sections (Å^2).

	$^2P_{3/2}\rightarrow{}^2P_{1/2}$		$^2P_{1/2}\rightarrow{}^2P_{3/2}$	
E_{tot}	E_{CM} (eV)	σ	E_{CM}	σ
0.90	0.411	0.35	0.233	1.24
1.145	0.656	0.64	0.478	1.78
1.435	0.946	1.09	0.768	2.84
1.650	1.161	1.55	0.983	3.88

IOSA is concerned, not only does it reproduce the experimental results reasonably well, but it also gives values very close to the TSH ones.[19] In Figs. 4(a) and 4(b), we give two results due to the previous IOSA version.[16] It is seen how they differ significantly from all other results.

In contrast to the results in Figs. 4(a) and 4(b), the fit between theory and experiment presented in Fig. 4(c) is somewhat less encouraging. The theoretical curves shows a stronger dependence on the energy than the experimental curves do, although all results seem to decrease as the energy decreases. This behavior is unexpected, because it hints at the existence of a potential barrier, which does not seem to exist for the initial $v^+ = 0,1$ states. We discuss this finding in greater detail in Sec. V.

B. Results for $Ar^+(^2P_j)+H_2\rightarrow ArH^+H$

Energy-dependent cross sections for $Ar^+(^2P_{3/2})$ and $Ar^+(^2P_{1/2})$ are shown in Figs. 5(a) and 5(b), respectively. Again, the theoretical results are compared with the experimental. In general, our experimental results fit the theoretical results much better than do those of Tanaka *et al.*[17,18] For both spin states, Tanaka *et al.*'s cross sections are not only larger than the others, but they also show a much stronger energy dependence. The more encouraging outcome of this comparison is the nice fit between our experimental and theoretical results for energies higher than 0.4 eV. Still, the different behavior at low energies is puzzling.

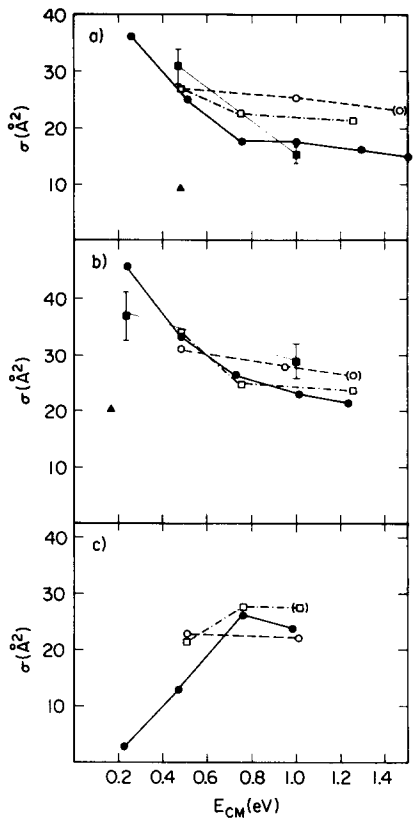

FIG. 4. Translational energy-dependent absolute cross sections for the exchange process $Ar+H_2^+(v^+)\rightarrow ArH^+ + H$. —●—, RIOSA results (present); ▲, RIOSA results (previous, Ref. 16); –■–, TSH results with error bars (Ref. 19); – –○– –, experimental results (present); –·–□–·–, experimental results (Ref. 17 and 18). (a) Results for $v^+ = 0$; (b) results for $v^+ = 1$; (c) results for $v^+ = 2$. Symbols between parentheses stand for linearly interpolated values with respect to next measured cross section.

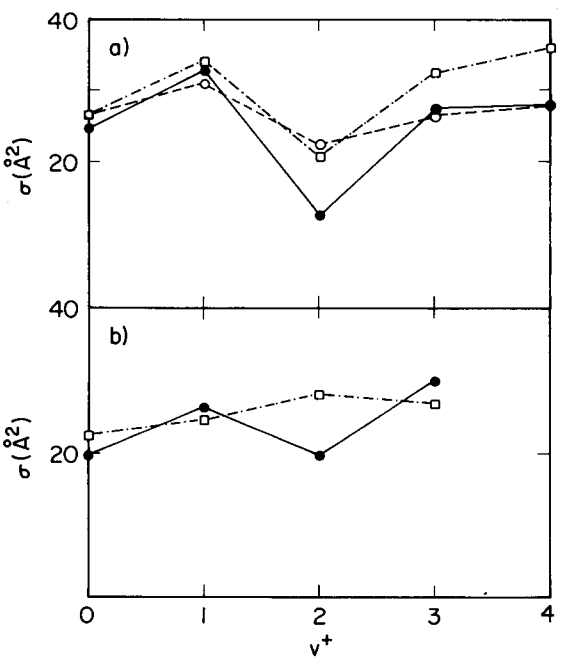

FIG. 3. Initial state-dependent total (absolute) cross sections for the exchange process $Ar+H_2^+(v^+)\rightarrow ArH^+ + H$. —●—, RIOSA results (present); –○–, experimental results (present); –·–□–·–, experimental results (Ref. 17 and 18). (a) Results for $E_{CM}\sim 0.48$ eV; (b) results for $E_{CM}\sim 0.75$ eV.

C. Results for $Ar+H_2^+(v^+)\rightarrow Ar^+(^2P_j)+H_2$

The cross sections for these charge transfer processes are presented in Tables IV and V and in Figs. 6–8.

Initially we discuss the charge transfer process in general, not distinguishing between the two spin states of Ar^+. The energy-dependent cross sections for $v^+ = 1$ and $v^+ = 2$ are shown in Figs. 6(a) and 6(b), respectively. In general, a reasonable fit between theory and experiment is obtained. This means that for $v^+ = 1$ the cross sections are small (2–6 Å^2), whereas for $v^+ = 2$ they are much larger (20–40 Å^2). However, whereas for $v^+ = 1$ we obtain the correct energy dependence, we fail to do so in the case of $v^+ = 2$. The reason maybe associated with the fact that $v^+ = 2$ is in resonance with $(v = 0, j = 1/2)$, and therefore the numerical results are much more sensitive to the details of the potential (which is semi-empirical, as mentioned

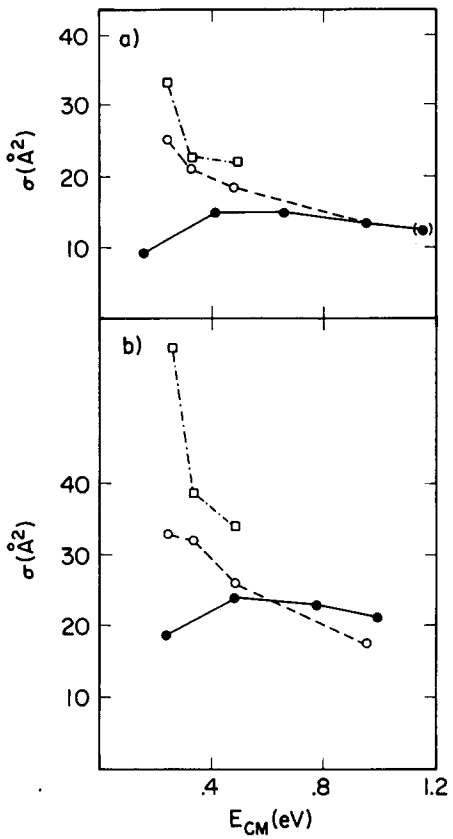

FIG. 5. Translational energy-dependent absolute cross sections for the exchange process $Ar^+(^2P_j) + H_2(v=0) \rightarrow ArH^+ + H$. Symbols as in Figs. 3. (a) Results for $j = 3/2$; (b) results for $j = 1/2$.

above). In Fig. 7 we present the dependence of the charge transfer cross sections on the initial vibrational states of H_2^+. The results for $E_{CM} = 0.46$ eV are presented in Fig. 7(a) and those for $E_{CM} = 0.75$ eV in Fig. 7(b). In Fig. 7(a), the IOSA results are compared with our experimental results as well as with those of Tanaka *et al.*,[17,18] while in Fig. 7(b), they are compared only with those of Tanaka *et al.* A nice agreement is shown in Fig. 7(a) (note that we show absolute, not relative, cross sections). A less encouraging fit is shown in Fig. 7(b), mainly due to the large cross sections at $v^+ = 2$. More detailed results are shown in Fig. 8, where we distinguish between the two final $Ar^+(^2P_j)$ states. The theoretical results are compared with our experimental values, which are the only ones available. Again, a nice fit is obtained.

D. Results for $Ar^+(^2P_j)+H_2(v=0) \rightarrow Ar+H_2^+(v^+)$

Results for these charge transfer processes are presented in Figs. 9 and 10. In Fig. 9 we show the energy-dependent cross sections for the two initial spin states of Ar^+. The theoretical cross sections are compared with our experimental values and with those of Henri *et al.*[28] In general, the agreement is good, namely, for $j = 3/2$ both theory and experiment yield small cross sections (less than 6 Å^2) and for $j = 1/2$ they yield larger cross sections (> 15 Å^2), but whereas for $j = 3/2$ the IOSA correctly reproduces the energy dependence of these cross sections, it fails to do so for the $j = 1/2$ case, where the steep increase of the cross sections as a function of the energy is not observed in the experiments.

The final vibrational distribution for the product ion H_2^+ for $E_{CM} = 1.0$ eV is presented for $j = 3/2$ in Fig. 10(a) and that for $j = 1/2$ in Fig. 10(b). Whereas the fit between experiment and theory is not satisfactory for $Ar^+(^2P_{3/2})$, a

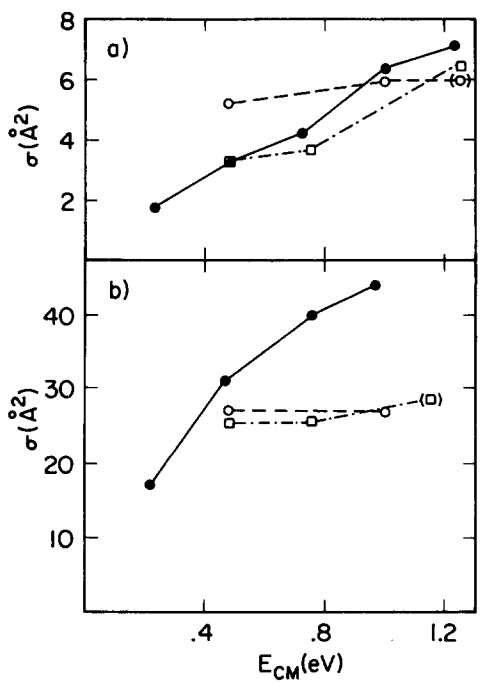

FIG. 6. Translational energy-dependent absolute cross sections for the charge transfer process $Ar + H_2^+(v^+) \rightarrow Ar^+ + H_2$. Symbols as in Fig. 3. (a) Results for $v^+ = 1$; results for $v^+ = 2$.

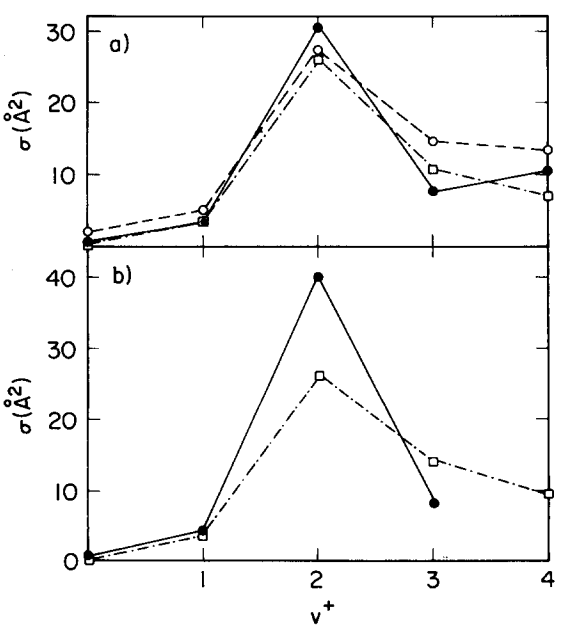

FIG. 7. Initial state-selected total absolute cross sections for the charge transfer process $Ar + H_2^+(v^+) \rightarrow Ar^+ + H_2$. Symbols as in Fig. 3. (a) Results for $E_{CM} = 0.48$ eV; (b) results for $E_{CM} = 0.75$ eV.

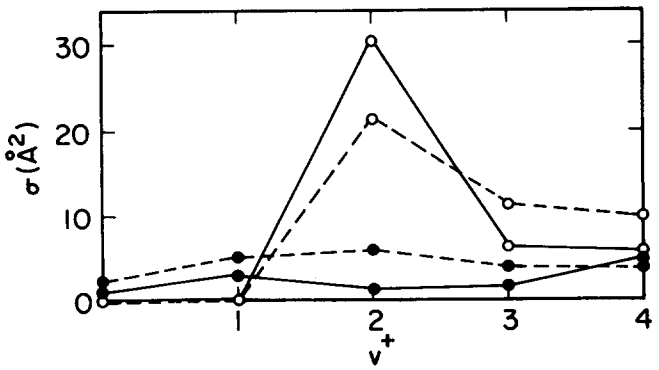

FIG. 8. State-to-state integral absolute cross section for the charge transfer process $Ar + H_2^+(v^+) \rightarrow Ar^+(^2P_j) + H_2$ as obtained for $E_{CM} = 0.48$ eV. —, RIOSA results; – – –, experimental results; ○, results for $j = 1/2$; ●, results for $j = 3/2$.

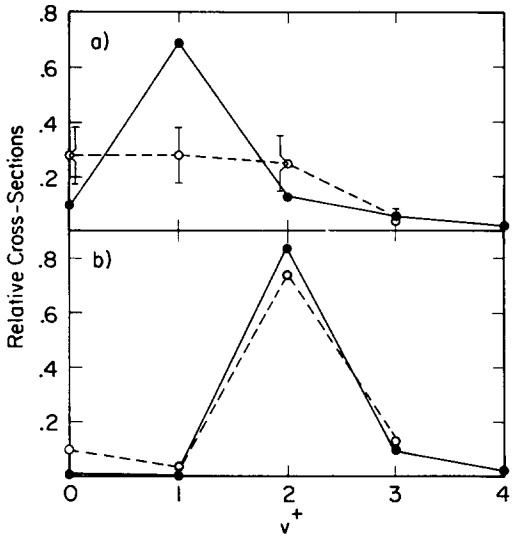

FIG. 10. Final vibrational distribution. Relative cross sections $(\sigma(j \rightarrow v^+)/\sigma(j \rightarrow \Sigma(v^+))$ for the charge transfer process $Ar^+(^2P_j) + H_2(v=0) \rightarrow Ar + H_2^+(v^+)$, as calculated at $E_{CM} = 1$ eV. —●—, RIOSA results (present); – –○– –, experimental results (present). (a) Results for $j = 3/2$; (b) results for $j = 1/2$.

nice agreement is obtained for $Ar^+(^2P_{1/2})$. One possible reason for the poor fit in the case of $j = 3/2$ could be the overall *small* cross sections in this case, which could lead to larger *experimental* errors.

E. Results for $Ar^+(^2P_{1/2}) + H_2(v=0) \leftrightarrows Ar^+(^2P_{3/2}) + H_2(v=0)$

Cross sections for spin transitions as a function of energy are presented in Fig. 11. Except for $E_{CM} = 1.2$ eV, experimental values are unavailable. Note that at this energy a good agreement is obtained for the endothermic process cross section $3/2 \rightarrow 1/2$, but the agreement is less than satisfactory for the reverse process. As for the energy dependence, measurements at higher energies (see Paper II) indicate that both cross sections increase. This finding is confirmed in the calculations.

V. DISCUSSION

A. The resonances

The dominant feature of the $(Ar + H_2)^+$ ionic system is the existence of vibronic resonance in the entrance (reagents) channel between $v = 0$ of the $Ar^+(^2P_{1/2}) + H_2$ system and the $v^+ = 2$ of the $Ar + H_2^+$ system. This situation is best described in Fig. 12, where we present vibronic curves, as a function of the translational coordinate R for the two $Ar^+(^2P_j) + H_2$ systems and the $Ar + H_2^+$ system. Note that, not only does the above-mentioned resonance [designated as (1/2,2)] exist in the asymptotic region, but it continues to smaller R values, where the diabatic couplings between the lower and the two upper surfaces become strong

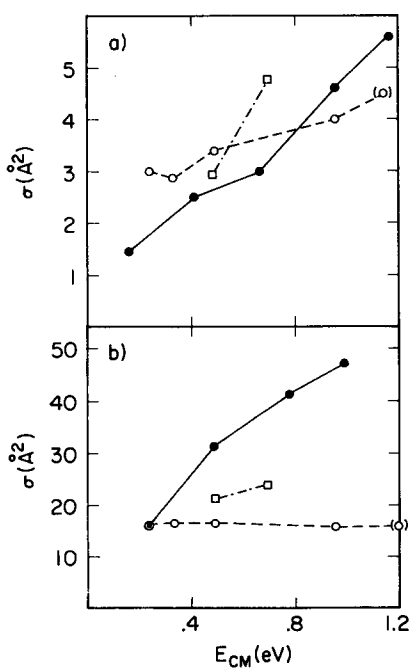

FIG. 9. Translational energy-dependent absolute cross sections for the charge transfer process $Ar^+(^2P_j) + H_2(v=0) \rightarrow Ar + H_2^+$. —●—, RIOSA results (present); – –○– –, experimental results (present); –·–□–·–, experimental results (Ref. 28).

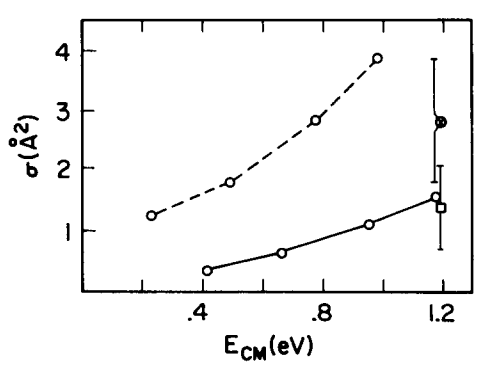

FIG. 11. Translational energy-dependent absolute cross section for the spin transition process $Ar^+(^2P_j) + H_2(v=0) \rightarrow Ar^+(^2P_j) + H_2^+$. —○—, RIOSA results for the $(3/2 \rightarrow 1/2)$ transition; –·–○–·–, RIOSA results for the $(1/2 \rightarrow 3/2)$ transition; □, experimental results for the $(3/2 \rightarrow 1/2)$ transition; ○, experimental result for the $(1/2 \rightarrow 3/2)$ transition.

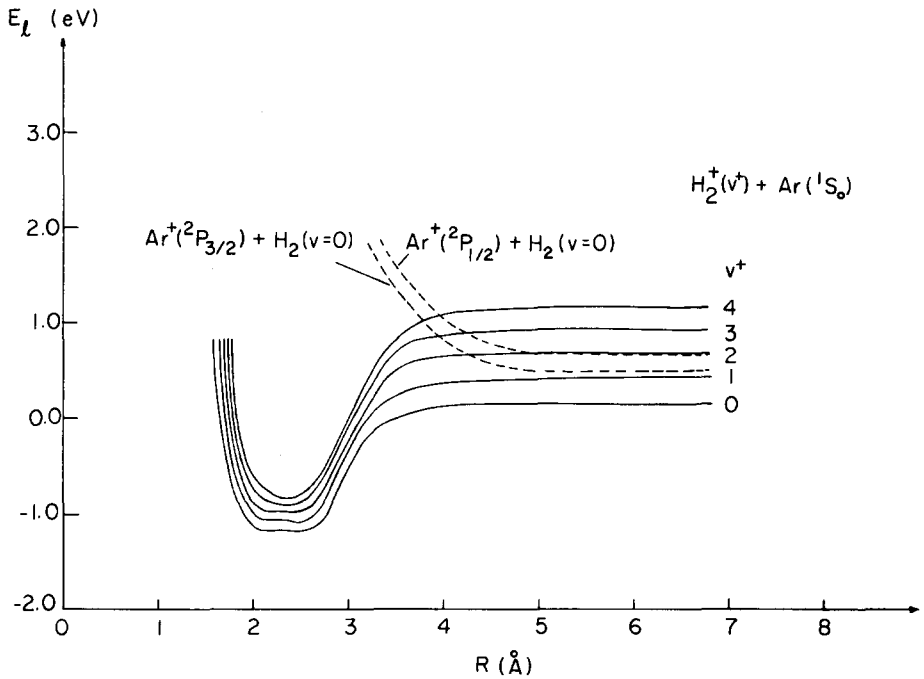

FIG. 12. Vibronic potential curves along the translational coordinate R for the three quasi-adiabatic potential energy surfaces. The calculations were carried out for $\gamma = 30°$; $r_{max} = 4$ Å, and $r_{min} = 0.3$ Å.

enough. Somewhat less pronounced is the resonance between the $Ar^+(^2P_{3/2}) + H_2(v=0)$ and the $Ar + H_2^+(v^+ = 1)$ [designated as (3/2,1)]. That the (1/2,2) resonance is much stronger than the (3/2,1) is due not only to the differences in the (asymptotic) energy gaps (0.019 eV vs 0.063 eV), but also to the fact that it continues to smaller R distances. Many of the results shown in the previous section, both in the figures and in the tables, support this observation.

At this point we examine the existence of the resonance from a different perspective. We calculated the differential cross sections, which are presented for $E_{tot} = 1.435$ eV in Fig. 13. In Fig. 13(a) we show differential cross sections for the two above-mentioned processes. For both we obtain strong forward scattering, but two main differences are apparent: (a) Whereas very clear rainbow scattering is seen in the (1/2,2) case, it seems not to be present in the (3/2,1) case. (b) The relative contribution of the forward angular range to the integral cross section is much larger for the (1/2,2) case. For instance, the contribution of the (0,30°) angular case in the (1/2,2) case is about 70%, whereas in the (3/2,1) case it is only 43%.

The importance of the resonance is seen mainly in Fig. 13(b), where we present the differential cross sections for the reactions $Ar + H_2^+(v^+ = 2) \rightarrow Ar^+(^2P_j) + H_2$ [designated as $(2,j)$]. For all practical purposes the (2,1/2) curve is identical to the (1/2,2) curve, which is another strong indication that these two states are strongly coupled. As an example of a nonresonance case, we show in the same figure the differential cross sections for the (2,3/2) case. Note that the strong forward region is nearly missing, and also that the rainbow shows up at a smaller angle, indicating a shallower potential well.

Experimental differential cross sections for the charge transfer process are hardly available and those that are available are not state-to-state cross sections. Still the cross sections relevant to ours seems to fit rather well, qualitatively, with our calculated cross sections:

(a) Hierl *et al.*[30] measured the differential cross section for the process:

$$Ar^+(^2P_{3/2,1/2}) + H_2 \rightarrow Ar + H_2^+ \qquad (V.1)$$

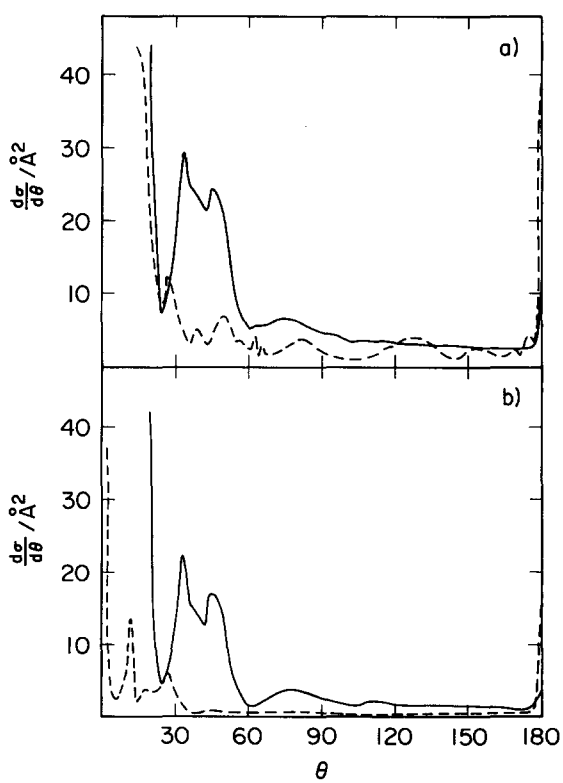

FIG. 13. State-to-state differential cross sections for the charge transfer process as calculated for E_{tot}-1.435 eV. —, Results for $j = 1/2$, – – –, results for $j = 3/2$. (a) $Ar^+(^2P_j) + H_2(v=0) \rightarrow Ar + H_2^+$; (b) $Ar + H_2^+(v^+ = 2) \rightarrow Ar^+(^2P_j) + H_2$.

and found, for the energy value $E_{CM} = 0.45$ eV (which is that closest to ours) essentially a similar distribution; namely, a strong forward peak in the angular range $0 \leqslant \theta_{CM} \leqslant 60$ and only minor contributions from the rest of the angular range.

(b) Bilotta *et al.*[31] measured the differential cross section for the reversed reaction

$$H_2^+ + Ar \rightarrow H_2 + Ar^+ (^2P_{1/2}, P_{3/2}), \qquad (V.2)$$

where the H_2^+ beam possesses, due to electron impact of H_2, the corresponding vibrational Franck–Condon distribution. For the translational energy $E_{CM} = 0.45$ eV, a dominant forward distribution is obtained (the authors labelled it "backward"), which again qualitatively fits ours.

However, whereas the calculated differential cross sections show a clear rainbow structure, this structure is lacking in the experimental cross sections. It is quite possible that since neither the initial nor the final states in the experiment are well selected, this structure, which is typical only for the resonantic transitions, is smeared out.

In Fig. 14 we present l-weighted opacity functions $(2l+1)\,P(E_t, l|\cdots)$, where $P(E_t, l|\cdots)$ is defined in Eq. (15). In Fig. 14(a) we present the opacity functions for $(Ar^+ (P_{1/2}), H_2)$ and in Fig. 14(b) those for $(Ar^+ (^2P_{3/2}), H_2)$. In each figure we show two curves, one for the exchange and the other for the charge transfer process. The most interesting pattern is that seen in Fig. 14(a) for the charge transfer process. The curve has at least three maxima: the largest maximum stands for the forward scattering, the next can be identified as responsible for the rainbow scattering, and the third, etc., are responsible for the supernumerary rainbows. A similar structure is obtained in Fig. 14(b), but its size is much smaller.

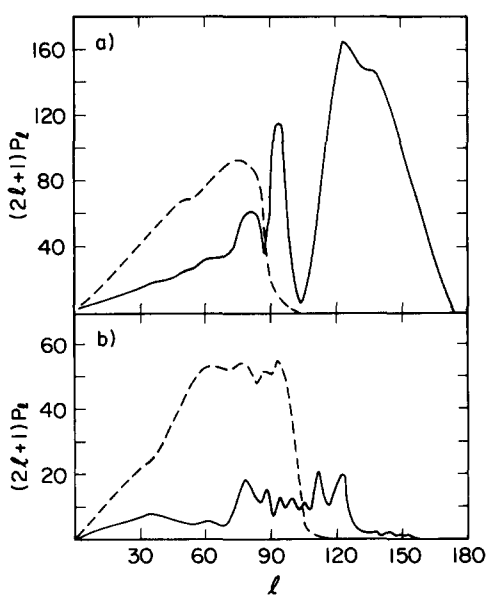

FIG. 14. l-weighted opacity functions ($(2l+1)P_l$) for charge transfer and exchange processes, as calculated for $E_{tot} = 1.435$ eV. —, $Ar^+ (^2P_j) + H_2(v=0) \rightarrow Ar + H_2^+$; – – –, $Ar^+ (^2P_j) \rightarrow H_2(v=0) \rightarrow ArH^+ + H$. (a) Results for $j = 1/2$; (b) results for $j = 3/2$.

B. Exchange versus charge transfer

The second feature which characterizes the $(Ar + H_2)^+$ system is the competition between charge transfer and exchange processes. This is best presented in terms of the l-weighted opacity functions shown in Fig. 14. Note that for the more resonant case, $Ar^+ (^2P_{1/2})$, the charge transfer process is not much affected by the exchange, because the charge transfer takes place mainly at the large l region, whereas the exchange occurs at the lower l region. However, since the charge transfer process is also relatively strong in the low l region, it competes directly with the reaction process and probably decreases the reactive cross sections. In the less resonant case, $Ar^+ (^2P_{3/2})$, the competition between the two processes is direct, both are affected, and probably this results in smaller cross sections compared to those without competition. This is expected to occur in all other cases, as is noticed from the reactive opacity functions presented in Fig. 15 for $E_{tot} = 1.435$ eV. All of these functions have a similar pattern with similar numerical values. The probabilities for $Ar^+ (^2P_{3/2}) + H_2$ are smaller because the calculated values are divided by two for symmetry considerations.

C. New IOSA versus old IOSA

Whereas the previous IOSA[16] treatment yields reactive cross sections which are too small, compared to both the experimental and the TSH results, the present version is seen to be significantly better. The comparison between the cross sections due to the three theoretical treatments is seen best in Fig. 4(a), where reactive cross sections for $v^+ = 0$ are presented. Whereas the TSH and the new IOSA cross sections are reasonably close, within the TSH error bar, the old IOSA result is more than three times smaller. A similar situation is encountered in Fig. 4(b) for $v^+ = 1$, but here the comparison between the present IOSA results and the previous TSH and IOSA results must be done more carefully, because the modification made in the potential matrix could affect the results. It is also important to emphasize that all the TSH results for $v^+ \geqslant 2$, as well as those for $Ar^+ + H_2$, are essentially obtained for a different potential, and therefore the comparison with the present IOSA results is meaningless.

To get more insight into the source of the differences

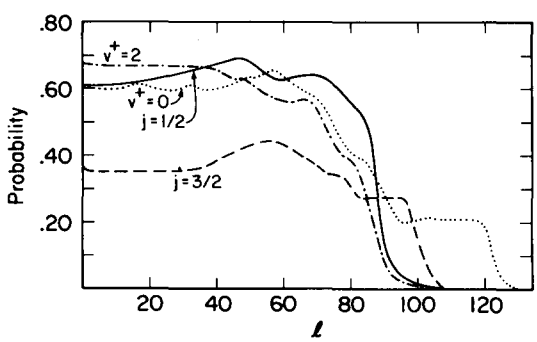

FIG. 15. Opacity functions for exchange processes as calculated at $E_{tot} = 1.435$ eV. v^+ stands for the process $Ar + H_2^+ (v^+) \rightarrow ArH^+ + H$. j stands for the process $Ar^+ (^2P_j) + H_2(v=0) \rightarrow ArH^+ + H$.

between the two IOSA treatments, we consider reactive (integral total) γ-dependent cross sections which are presented in Fig. 16 for $v^+ = 0$. Two curves are shown, one due to the previous treatment calculated at $E_{tot} = 0.6$ eV and the present one calculated at $E_{tot} = 0.65$ eV.

The results are more than surprising. *A priori*, we would expect that the $\gamma = 0$ (the collinear) results in the two treatments would be the same and that differences, if found at all, would be at higher values of γ. In fact, the converse happens. However, we know from previous studies that for a "pure" collinear case[6(a),9] (namely for $l_\lambda = l_\nu = 0$) both the ordinary reactive treatment and the treatment which utilizes the optical potentials give identical results. Thus, the differences between the results obtained with the two ($\gamma = 0$) treatments should be attributed to the transformation of the angular momenta. In all previous RIOSA treatments (for both the quantum and the classical) we made two assumptions:

(a) The angular kinetic energy down to the matching line in the reagents arrangement λ is given by

$$E^{\lambda}_{ang} = \frac{\hbar^2}{2\mu R^2_\lambda} l_\lambda (l_\lambda + 1), \tag{19}$$

and that from the matching line outwards into the products arrangement is given by

$$E^{\nu}_{ang} = \frac{\hbar^2}{2\mu R^2_\nu} l_\nu (l_\nu + 1). \tag{19'}$$

(b) The exchange between l_λ and l_ν is done along the matching line and consequently, for a given l_λ, the value of l_ν is determined by assuming these two expressions to be identical on the matching line, where the ratio (R_λ/R_ν) is known.

In the new IOSA version, no transformation of angular momentum is encountered and consequently Eq. (19) is assumed to hold along the whole space configuration treated.

We complete this section by showing a few additional γ-dependent reactive cross sections and charge transfer cross sections which are presented for $E_{tot} = 0.9$ eV in Figs. 17(a) and 17(b), respectively. The reactive cross sections for the two lowest vibrational states exhibit strong dependence on γ, similarly to those shown previously. A much milder dependence on γ is obtained for three other cases calculated for initial states which are strongly affected by the electronical nonadiabatic couplings. The conclusion of this is that the nonadiabatic couplings, which are known to be only weakly dependent on γ,[16] are so dominant that other effects become secondary. Consequently the dependence of the various cross sections on γ tends to disappear.

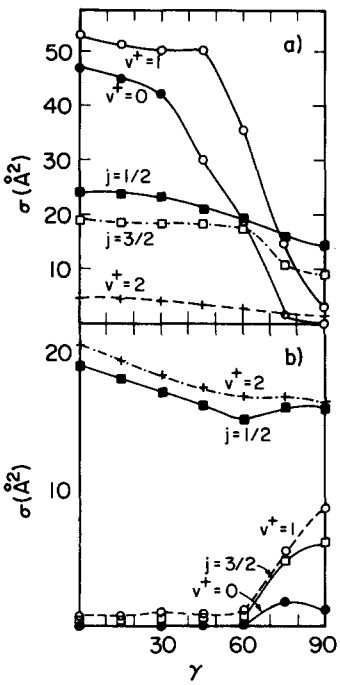

FIG. 17. γ-dependent cross sections as calculated at $E_{tot} = 0.9$ eV. (a) Exchange processes; (b) charge transfer processes. v^+ stands for the reagents $Ar + H_2^+(v^+)$; j stands for the reagents $Ar^+(^2P_j) + H_2(v=0)$.

As for the charge transfer process, again a mild dependence on γ is obtained for the two resonance cases, whereas the cross sections for the other initial states show a stronger γ dependence. The fact that these cross sections increase as γ approaches 90° could be a direct outcome of the strong decrease in the exchange rate. It is important to indicate that a similar behavior was encountered in our previous IOSA study, although the potentials are significantly changed by introducing the two spin states of Ar^+.

It should also be indicated that charge transfer differential cross sections calculated within the two versions of the RIOSA are similar.

VI. SUMMARY

In this work we have carried out an extensive study for the $(Ar + H_2)^+$ system. The present treatment differs from that previously published in three respects:

(1) In the previous study, the two spin states of Ar^+, which are known to have a dominant effect on the various reactive and charge transfer cross sections, were assumed to be degenerate. Consequently, the numerical treatment was carried out employing two potential energy surfaces. In the present study, this deficiency is corrected and the calculations are performed with three surfaces, of which the higher two correlate with the spin states of Ar^+.

(2) In the present study we employ a new version of the reactive IOSA, which avoids the transformation from reagents to products coordinates. According to this version the reactive system is treated as an extended inelastic system, with optical potentials substituted at the entrances of all products arrangements, to absorb the outgoing fluxes. The

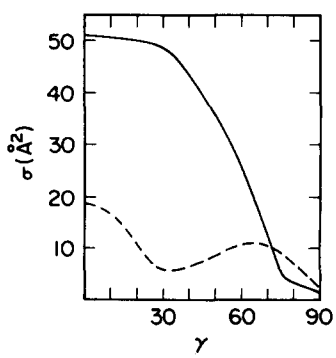

FIG. 16. γ-dependent exchange cross sections for the process $Ar + H_2^+(v^+ = 0) \rightarrow ArH^+ + H$.—, present RIOSA for $E_{tot} = 0.65$ eV; – – –, previous RIOSA for $E_{tot} = 0.60$ eV.

resulting coupled Schrödinger equations are solved without difficulties, employing the ordinary propagation method.

(3) In the present study an extensive numerical treatment is carried out for six total energies in the range $0.4 \leqslant E_{tot} \leqslant 1.65$ eV. Three different processes are treated simultaneously: exchange, charge transfer, and spin transitions. The initial state-selected total integral cross sections for exchange are compared with both experimental results and TSH calculations. In most cases a very good agreement is obtained (in particular with the TSH results, whenever the comparison was feasible). The state-to-state charge transfer and spin transition integral cross sections are compared with experimental results and, again, in most cases good agreement is obtained. In particular, the calculations verify the dominant role of the resonance between the $Ar + H_2^+(v^+ = 2)$ state and the two $Ar^+(^2P_j) + H_2(v = 0), j = 1/2,3/2$ states. Unfortunately, the largest discrepancy is obtained for the most resonant transition, $(1/2,0) \rightarrow (v^+ = 2)$. The strong energy increase of the calculated cross sections is not observed in the experiment, although the numerical absolute magnitudes are reasonably close. In addition to these calculations, the numerical treatment contains differential cross sections, opacity functions, and steric factors.

ACKNOWLEDGMENTS

This work is supported by the National Science Foundation Grant No. CHE 8913282. Acknowledgment is also made to the donors of the Petroleum Research Fund, administered by the American Chemical Society, for the partial support of this research. The theoretical computation is made possible by a grant from the Computer Center of Iowa State University and a grant from the Director Development Fund of the Ames Laboratory. One of us (M.B.) would like to thank Dr. J. Coyle, J. Hoekstra, and J. Calsyn of the Iowa State University Computer Center for their assistance during the calculations.

[1]C.-Liao, R. Xu, G. D. Flesch, M. Baer, and C. Y. Ng, J. Chem. Phys. **93**, 4818 (1990) (referenced as Paper I).
[2]C.-L. Liao, R. Xu, S. Nourbakhsh, G. D. Flesch, M. Baer, and C. Y. Ng, J. Chem. Phys. **93**, 4832 (1990) (referenced as Paper II).
[3]D. Neuhauser and M. Baer, J. Chem. Phys. **90**, 4351 (1989).
[4]D. Neuhauser and M. Baer, J. Phys. Chem. **93**, 2862 (1989); J. Chem. Phys. **91**, 4651 (1989).
[5]D. Neuhauser, M. Baer, R. S. Judson, and D. J. Kouri, J. Chem. Phys. **90**, 5882 (1989); **93**, 312 (1990).
[6](a) D. Neuhauser and M. Baer, J. Phys. Chem. **94**, 185 (1990); (b) J. Chem. Phys. **92**, 3419 (1990).
[7]R. S. Judson, D. J. Kouri, D. Neuhauser, and M. Baer, Phys. Rev. A (in press).
[8]M. Baer, D. Neuhauser, and Y. Oreg, J. Chem. Soc. Faraday Trans. **86**, 1721 (1990).
[9]D. Neuhauser, M. Baer, and D. J. Kouri, J. Chem. Phys. (in press).
[10]The propagation of the S matrix is probably very similar to that of the R matrix, see J. C. Light and R. B. Walker, J. Chem. Phys. **65**, 4272 (1976).
[11](a) V. Khare, D. J. Kouri, and M. Baer, J. Chem. Phys. **71**, 1188 (1979); (b) J. Jellinek and M. Baer, *ibid.* **76**, 4883 (1982); H. Nakamura, A. Ohaski, and M. Baer, J. Phys. Chem. **90**, 6176 (1986).
[12]J. M. Bowman and K. T. Lee, J. Chem. Phys. **72**, 5071 (1980).
[13]G. D. Barg and G. Drolshagen, Chem. Phys. **47**, 209 (1980); D. C. Clary and G. Drolshagen, J. Chem. Phys. **76**, 5027 (1982); D. C. Clary, Chem. Phys. **71**, 117 (1982); **81**, 379 (1983); C. E. Dateo and D. C. Clary, J. Chem. Soc. Faraday Trans. 2 **85**, 1685 (1989).
[14]B. M. D. D. Jensen op de Haar and G. G. Balint-Kurti, J. Chem. Phys. **85**, 329 (1987); **90**, 888 (1989).
[15]H. Nakamura, Phys. Reps. (in press); H. Nakamura, J. Chem. Phys. **90**, 4835 (1989).
[16]M. Baer and H. Nakamura, J. Chem. Phys. **87**, 4651 (1987); M. Baer, H. Nakamura, and A. Ohsaki, Chem. Phys. Lett. **131**, 468 (1986); M. Baer and H. Nakamura, J. Phys. Chem. **91**, 5503 (1987).
[17]K. Tanaka, J. Durup, T. Kato, and I. Koyano, J. Chem. Phys. **74**, 5561 (1981).
[18]K. Tanaka, T. Kato, and I. Koyano, J. Chem. Phys. **75**, 4941 (1981).
[19]S. Chapman, J. Chem. Phys. **82**, 4033 (1985). A few of the lower energy cross sections were obtained by private communication.
[20]M. Baer, C. Y. Ng, and D. Neuhauser, Chem. Phys. Lett. **169**, 1534 (1990).
[21]L. Munchick and E. A. Mason, J. Chem. Phys. **35**, 1671 (1961); K. Takayanaki, Progr. Theor. Phys. (Kyoto), Suppl. **25**, 40 (1963); K. Kramer and R. B. Bernstein, *ibid.* **44**, 4473 (1964); C. F. Curtiss, *ibid.* **49**, 1952 (1968); T. P. Tsien, G. P. Parker, and R. T. Pack, *ibid.* **59**, 5373 (1973); D. Secrest, *ibid.* **62**, 710 (1975); V. Khare, D. J. Kouri, and D. K. Hoffman, *ibid.* **74**, 2275 (1981); M. A. Wartel and R. J. Cross, *ibid.* **55**, 4983 (1971); J. M. Bowman and J. Arruda, Chem. Phys. Lett. **41**, 43 (1976); R. Schinke and P. McGuire, Chem. Phys. **28**, 129 (1978); R. D. Levine, Chem. Phys. Lett. **4**, 24 (1969); M. A. Brandt and D. G. Truhlar, *ibid.* **23**, 48 (1973).
[22]M. Baer, G. Niedner-Schatteburg, and J. P. Toennies, J. Chem. Phys. **88**, 1461 (1988); **91**, 4169 (1989).
[23]F. A. Gianturco, A. Palma, E. Semprini, F. Stefani, and M. Baer, Phys. Rev. A (in press); G. Parlant and E. A. Gislason, J. Chem. Phys. **91**, 5359 (1989); V. Sidis, D. Grimbert, M. Sizun, and M. Baer, Chem. Phys. Lett. **163**, 19 (1989).
[24]P. J. Kuntz and A.C. Roach, J. Chem. Soc. Faraday Trans. **268**, 259 (1972).
[25]M. Baer and J. A. Beswick, Chem. Phys. Lett. **51**, 369 (1977); Phys. Rev. A **19**, 1559 (1979); M. Baer, Molec. Phys. **35**, 1637 (1978).
[26]M. Baer, J. Jellinek, and D. J. Kouri, J. Chem. Phys. **78**, 2962 (1983).
[27]Y. C. Zhang, Z. H. Zhang, D. J. Kouri, and M. Baer, Chem. Phys. **114**, 267 (1987); M. Baer, *ibid.* **123**, 365 (1988); I. Last, S. Ron, and M. Baer, Isr. J. Chem. **29**, 451 (1989).
[28]G. Henri, M. Lavallee, O. Dutuit, J. B. Ozenne, P. M. Guyon, and E. A. Gislason, J. Chem. Phys. **88**, 6381 (1988).
[29]F. A. Houle, S. L. Anderson, D. Gerlich, T. Turner, and Y. T. Lee, J. Chem. Phys. **77**, 748 (1982); Chem. Phys. Lett. **82**, 392 (1981).
[30]P. M. Hierl, V. Pacak, and Z. Herman, J. Chem. Phys. **67**, 2678 (1977).
[31]R. M. Bilotta, F. N. Preuninger, and J. M. Farrar, Chem. Phys. Lett. **74**, 95 (1980).